Modeling of Coupled Mass and Heat Transfer Through Venting Membranes for Automotive Applications

Amine Barkallah
Institut Européen des Membranes, ENSCM, CNRS, UMII, Université de Montpellier II, CC047, 2 Place Eugène Bataillon, Montpellier 34095, Cedex 5, France, and
Technocentre Renault, 1 Avenue du Golf, Guyancourt Cedex 78288, France

Johana Mörée, Jose Sanchez, and Stephanie Druon Bocquet
Institut Européen des Membranes, ENSCM, CNRS, UMII, Université de Montpellier II, CC047, 2 Place Eugène Bataillon, Montpellier 34095, Cedex 5, France

Jean Rivenc
Technocentre Renault, 1 Avenue du Golf, Guyancourt Cedex 78288, France

DOI 10.1002/aic.11689
Published online December 24, 2008 in Wiley InterScience (www.interscience.wiley.com).

Experimental and theoretical approaches based on a mathematical model, have been developed to study the evolution of environmental parameters (temperature, total pressure, relative humidity, and water vapor partial pressure) inside a housing of an electronic device with a window containing a macroporous membrane. The model was based on the coupling of mass and heat transfer taking into account the effects of polarization of concentration in boundary layers. Membranes have been characterized by mercury porosimetry, liquid entry pressure measurements, scanning electron microscopy, and gas permeation. Once the model was experimentally validated, it was applied to investigate the influence of membranes on heat and mass transfer and to study the impact of the boundary layers on the global mass transport. The results demonstrated the importance of the membrane choice and dimensions to get the best temperature regulation and avoid water condensation inside an automotive electronic control unit (ECU).
 AIChE J, 55: 294–311, 2009
Keywords: venting membrane, coupled mass and heat transfer, modeling, polymer hydrophobic membrane, characterization methods

Introduction

The study of mass and heat exchanges between differently shaped enclosures and the environment are becoming more and more extensive because this coupled transfer has wide application domains like on passive protection of electronic equipment, energy conservation in buildings, solar energy collection etc. In many cases, like on the protection of electronic devices, it is very important to control carefully these heat and mass exchanges through the enclosure surface. Usually the protection enclosures are made on solid and dense materials that have a limited capacity to exchange with surroundings. This characteristic can be prejudicial when quick changes in gas composition or temperature inside or outside the enclosure need a rapid response. In such cases, porous membranes can be used to partially substitute the exchange surface to accelerate, control, and quantify heat exchanges and mass transfer.

Automotive electronic devices or electronic control units (ECU) are usually placed inside an enclosure, indeed, a good

Correspondence concerning this article should be addressed to Jose Sanchez at sanchez@iemm.univ-montp2.fr.

knowledge and control of the influence of environmental parameters (temperature, pressure, and humidity) is very important for their right operation. In fact, in nowadays vehicles, multiple functions are controlled electronically and some modern cars can have up to 30 electronic ECU's to manage all vital, security, and comfort systems. Some ECU's are placed in the engine compartment and are often exposed to extreme conditions because of electronic heat dissipation, weather condition changes, water splashes, or complete immersion in some driving conditions.

ECU's are normally enclosed in a metallic or plastic hermetically sealed box to protect it from the surrounding fluids (liquids and gases). The limitation of this solution are the pressure changes in the box which are essentially the result of temperature changes due to normal electronic working conditions or external heat sources such as engine heat dissipation, solar energy accumulation etc. In fact, these phenomena lead to mechanical strains on the sealing and on the box material itself, leading to a possible loss of reliability.

The use of hydrophobic macroporous membranes, which can let air pass and prevent all liquids from passing through, is a solution to this problem. Nevertheless, these membranes are not selective to water vapor transfer (macroporous membranes have pores with mean pores size higher than 50×10^{-9} m) and can lead to water condensation in the case of rapid temperature decrease after a long exposition to high values of relative humidity (RH).

For the reasons exposed earlier, it is very important to have a good knowledge of the evolution of mass and heat transfers inside such electronic devices to quantify the impact of a membrane in such devices under normal or extreme environmental conditions. For this purpose, the development of models coupling mass and heat transfers is necessary to understand the evolution of internal parameters, such as temperature, pressure, and RH variation during a car typical use conditions.

In the heat transfer domain, different previous studies have been done and these works are classified according to the type of the enclosure, its orientation, the existence of a vent, the type of the heat source and its location.

Ostrach[1] and Catton[2] provided large reviews of the literature and an extensive bibliography on natural convection in different geometrical enclosures with different orientations. Yu and Joshi[3] and Nada and Moawed[4] paid more attention to the impact of the presence of vent slots on the heat transfer and on internal fluid velocities. These works have been done with different heat source positions and forms and with different contribution of the walls to heat dissipation (adiabatically isolated, isothermal walls, etc).

Other works have been done to study gas permeation and heat transfer in porous media and especially in membranes. Khayet et al.[5] studied heat and mass transfer through a hydrophobic polymeric membrane separating two liquid phases where the mass transfer is taking place by evaporation of the first liquid phase (distillate) and diffusion under partial vapor pressure difference through the membrane pores. They studied also the sweeping gas membrane distillation process where permeate is swept by a gas flow.[6] Other similar membrane processes with macroporous and hydrophobic membranes like osmotic evaporation, membrane extraction or evaporation have been studied by our group.[7–10] In these previous works mass and heat transfer models have been built taking in consideration the operating parameters and the structural characteristics of membranes. In some cases, a good knowledge of these structural characteristics is difficult to be determined experimentally and only the coupling of experiments and modeling is able estimating them.

Beuscher and Gooding,[11] Mourgues and Sanchez[12] and Martinez et al.[13] studied experimentally and numerically the gas permeation through porous membranes. They have contributed to the characterization of porous membranes by identifying the mass transfer parameters. They investigated different types of mono-layered membranes by experiments of steady-state gas permeation, isobaric diffusion and transient diffusion to obtain the parameters of the dusty gas model (DGM).[14] This approach was extended to multilayer porous membranes. Isothermal conditions are often assumed in these studies, even if thermal effects are recognized as an important issue in some models of transfer through membranes.

Gibson[15] studied the effect of the temperature on water vapor transport through polymer membrane laminates used for breathable clothes and roof protections. Hussain et al.[16] have also studied the heat and mass transfer in tubular ceramic membranes for membrane reactors to consider all the parameters which can have an impact on the membrane performance.

The main objective of this work was to build up a model of mass and heat transfer in an enclosure which has a part of its surface covered with a macroporous and hydrophobic membrane. This enclosure or electronics housing is placed in environmental conditions which are representative of automotive working conditions with variations of temperature, RH, total pressure, and partial water vapor pressure (Figure 1). The housing contains also a printed circuit board (PCB) that includes a source of heat.

Firstly, this work starts with the characterization of different commercial macroporous and hydrophobic membranes to determine the main relationships between the membrane structure and mass transport parameters used as modeling inputs. Secondly, a model was established, starting from general heat and mass transport equations and coupling them by taking into account their reciprocal dependences. Thirdly, simulation results were compared, for different environmental conditions, to the experimental data obtained with two different enclosures to validate the model.

Finally, we studied the impact of some parameters of the system on heat and mass transfer fluxes to choose the best parameters related to both, membrane structure and housing design. All these rules will be added to the existing Renault-Nissan specification book in a near future.

Experimental Methods

Membranes

Morphological and structural parameters were characterized by different techniques for six different commercial flat sheet hydrophobic membranes provided by three different membrane manufacturers (W.L Gore, Pall, and Nitto Denko). These membranes presented different morphologies and structures and were all made of polymers, have hydrophobic properties and presented mean pores sizes in the range of macropores (higher than 5.0×10^{-8} m). Table 1 summarizes the different types of membranes used in this work.

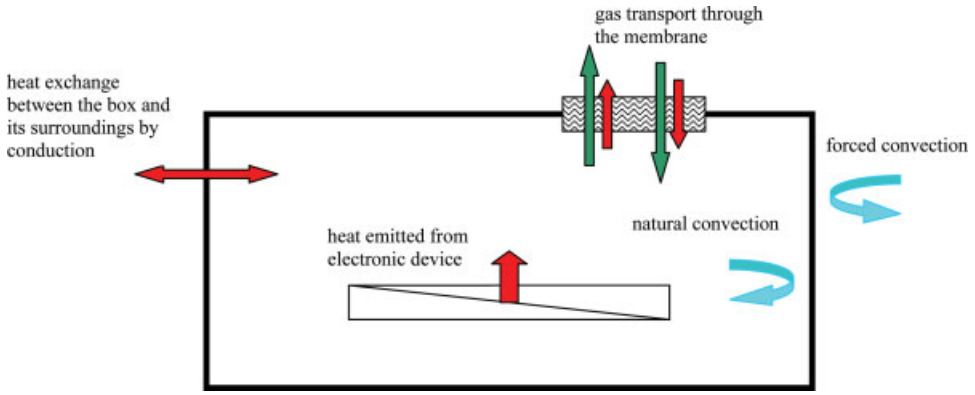

Figure 1. Schematic representation of the enclosure or protecting box equipped with a membrane and a printed circuit board.

[Color figure can be viewed in the online issue, which is available at www.interscience.wiley.com.]

Membranes characterization

Membranes have been characterized by different techniques like scanning electron microscopy (SEM) (Hitachi S-4500 I microscope), mercury porosimetry (Autopores II-9215 Micromeritics) and liquid entry pressure (LEP) which was used to study the membranes hydrophobicity.[17,18] LEP measurements were carried out in a home-made apparatus. A detailed description of the apparatus and methodology used here has been already published by our group.[19] Finally, nitrogen permeation experiments were carried out in a Wilcke-Kallenback cell working on sweep gas conditions. Retentate and permeate sides pressures were continuously monitored by the help of very sensitive pressure transducers (Keller PR23) (±50 Pa). The cell was placed in a temperature-controlled chamber and permeation was measured at 25°C ± 1°C at very low transmembrane pressures (ranged between 0 Pa and 9000 Pa) to determine the contribution of different mass transport mechanisms: slip flow, diffusion, and convection. Results are presented in the third section.

Experimental set-up with an actual electronics housing

Experiments were carried out placing the electronic housing in a climatic chamber (Heraeus Vötsch HC 7020). This chamber allows establishing very quickly (step variation) stable environmental conditions (temperature and RH) by using a fan inside (air velocity ~4 m s^{-1}). The experiments were carried out as follows: the housing (inside and outside) was equilibrated at initial room conditions (temperature and RH) and outside conditions were changed quickly by placing the tested box directly in the stabilized climatic chamber through a by-pass. The climatic chamber was connected to its surrounding with the help of opening slots so we can consider that its internal pressure was equal to the atmospheric one.

A first series of experiments were carried out using an existing electronic housing currently used to control automatic gear boxes (AISIN SU1) and which is represented in Figure 2. This aluminum alloy housing dimensions were: (164 × 10^{-3}-m length) × (86 × 10^{-3}-m width) × (40 × 10^{-3}-m height) (however, the thickness was not homogeneous and an approximate mean value of 2 × 10^{-3} m was considered). For practical reasons (simulation of the heat emitted by a PCB) in this series of experiments four resistances (Sfernice RH10 4.7 Ω) were placed inside the box to generate heat. The resistances were installed on a metallic board fixed to the inner part of the metallic housing. The metallic board dimensions were (108 × 10^{-3}-m length) × (50 × 10^{-3}-m width) × (1.35 × 10^{-3}-m thickness). Two RH sensors (Honeywell HIH-3601 with an accuracy of 2% in a full scale of non condensing 0–100%) were placed inside and outside the box and as close as possible to the membrane location to follow the evolution of the water vapor concentration during experiments. A pressure sensor [Honeywell 26 PC with an accuracy of 0.5% of the full working range

Table 1. Tested Membranes

Membrane	Material	Support
1	Expanded PTFE	No
2	Expanded PTFE	Yes (PA)
3	Expanded PTFE	Yes (PP)
4	Expanded PTFE	Yes (PP)
5	Acrylic polymer	Yes (PA)
6	Acrylic polymer	Yes (PA)

PA, Polyamide; PP, Polypropylene.

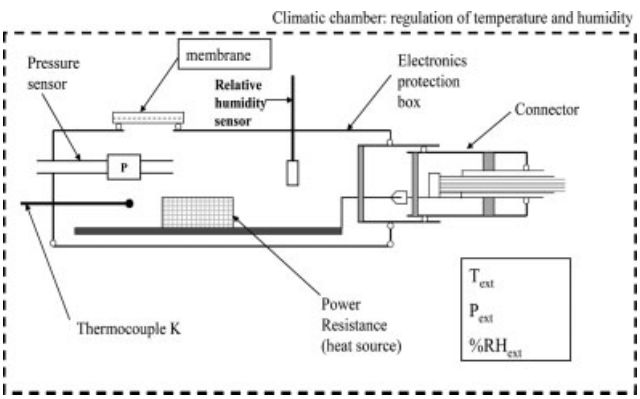

Figure 2. Scheme of the actual studied electronic box placed in a controlled atmosphere and equipped with different sensors.

(0–10^5 Pa)] was placed inside the enclosure. In this series of experiments, the membrane used corresponds to the number 4 in Table 1 and 5.02×10^{-5} m^2 of this membrane were placed on the upper side of the box. The edges were sealed with silicon glue (Loctite Silicomet JS 544) to avoid leaks.

All the sensors data were recorded using a multimeter Keithley 2700.

Two different experiments were carried out; they correspond to existing test cases in automotive applications:

- Maximum electronics heat dissipation (corresponding to a Diesel Engine Control Unit): equivalent to 25 W and ambient outside parameters (25°C, 45% RH).
- Maximum temperature of engine compartment with nondissipating electronics and very high humidity level, these conditions can also be considered as aging conditions used for automotive electronics and housings testing (85°C, 85% RH).

As far as this device is an actual housing for automotive electronics industry, some parameters (alloy composition, thickness, etc) were difficult to be determined precisely. This problem was by-passed carrying out a second series of experiments with a home-made box with well-known parameters (like type of alloy, homogeneous thickness, simple geometry etc).

This second reference box was used to carry out further validation experiments; it was made of 316 stainless steel and had well-known calibrated dimensions: 160-mm length, 100-mm width, and 40-mm height with a homogeneous thickness of 4 mm. This box did not contain a PCB or resistances placed inside. The used membrane was the same used for the first actual housing (membrane 4) but had a bigger surface of 3.14×10^{-4} m^2.

The experimental results obtained with this box will be presented in the fifth section.

Membranes Characterization Results

As explained earlier in the introduction, membrane characterizations are necessary first to determine if such commercial membranes are adapted to our application and secondly to determine some structural parameters which are necessary for the calculations that will be carried out with the developed model.

Electron micrographs

Microscopic observations of the surface and the cross section of four of the membranes studied here are shown in Figure 3. In this Figure we can observe the surface (3a, 3c, 3e, 3g) and the cross section (3b, 3d, 3f, 3h) of membrane 1: (3a, 3c), membrane 2: (3c, 3d), membrane 3: (3e, 3f) and membrane 5: (3g, 3h). Membrane 4 and 6 are not shown here because they have the same structure than membranes 3, 2, and 5, respectively. We can observe that we have different types of structure, the first one is represented by membrane 1 (3a and 3b) which is made of a monolayer of expanded PTFE. This type of membrane is made by one directional PTFE extension process allowing a good control of the pore size and the porosity. Membranes 2–4 (Figures 3c–f) have a support which provides the mechanical resistance and one or two separative layers. We can notice here that expansion process for the manufacturing of separative layers was probably carried out in different directions allowing obtaining a porous structure with a less precise control of mean pores size and porosity.

Membranes 5 and 6 (3g, 3h) have different structure and manufacturing process as the active layer is embedded in the polyamide support facing then some stability problems at the interface support-active layer.

Mercury intrusion method

Table 2 summarizes the results obtained with the mercury intrusion method. The mean pores size and the porosity have been used for the modeling. We can notice that all pore sizes are in the range of macroporosity (mean pores size higher than 5.0×10^{-8} m) with a very high porosity characteristic of this type of fibrous structure.

Liquid entry pressure

Table 3 summarizes the results of LEP obtained using distilled water for the tested membranes and the estimated pore diameter calculated by the Washburn equation.[18,19] The results shown in Table 3 confirm the order of magnitude obtained with mercury pressure intrusion measurements (Table 2). However, we can observe that the estimated pore diameter using the water intrusion method is a little higher than the mean pores size obtained by mercury porosimetry because in liquid permeation we mostly observe the contribution of the larger pores. We can observe that all these membranes would be used in automotive electronics housing venting application because the specifications for the industry [Membrane supplier data sheets (Nitto Denko: NTF series, Pall: Versapor series, and W. L Gore: Membrane vents)] impose a minimum LEP of 60,000 Pa.

Permeation results

Figure 4 presents nitrogen permeation results as a function of transmembrane pressure for membrane 1 at three different temperatures (25, 40, and 60°C). The particular shape of the curves with a first important decrease followed by a small increase of the permeance with the pressure is classical of a mixed contribution of different gas transport phenomena: Knudsen and molecular diffusion, slip flow phenomena and convection in macroporous materials at very low applied transmembrane pressures. Scott and Dullien[20] and Dullien[21] have also reported this kind of behavior and determined an equation based on the contribution of three different transport theories: the Hagen-Poiseuille equation, the theory of gas diffusion in porous media and the gas kinetic theory. At ΔP close to 0 Pa the experimental and theoretical curves intercept the ordinate axis at the corresponding flow rate of pure diffusion flow (molecular + Knudsen, with relative contributions depending on the mean free path). The transition region results normally of a contribution of diffusion slip flow and convection, whereas in the last part (linear) the mass transport is mainly due to convection (Hagen-Poiseuille contribution). Their mathematical treatment resulted in simulation curves matching well experimental results; however it was difficult from their theory to obtain, in an explicit form, some parameters of porous media like porosity and tortuosity. Other

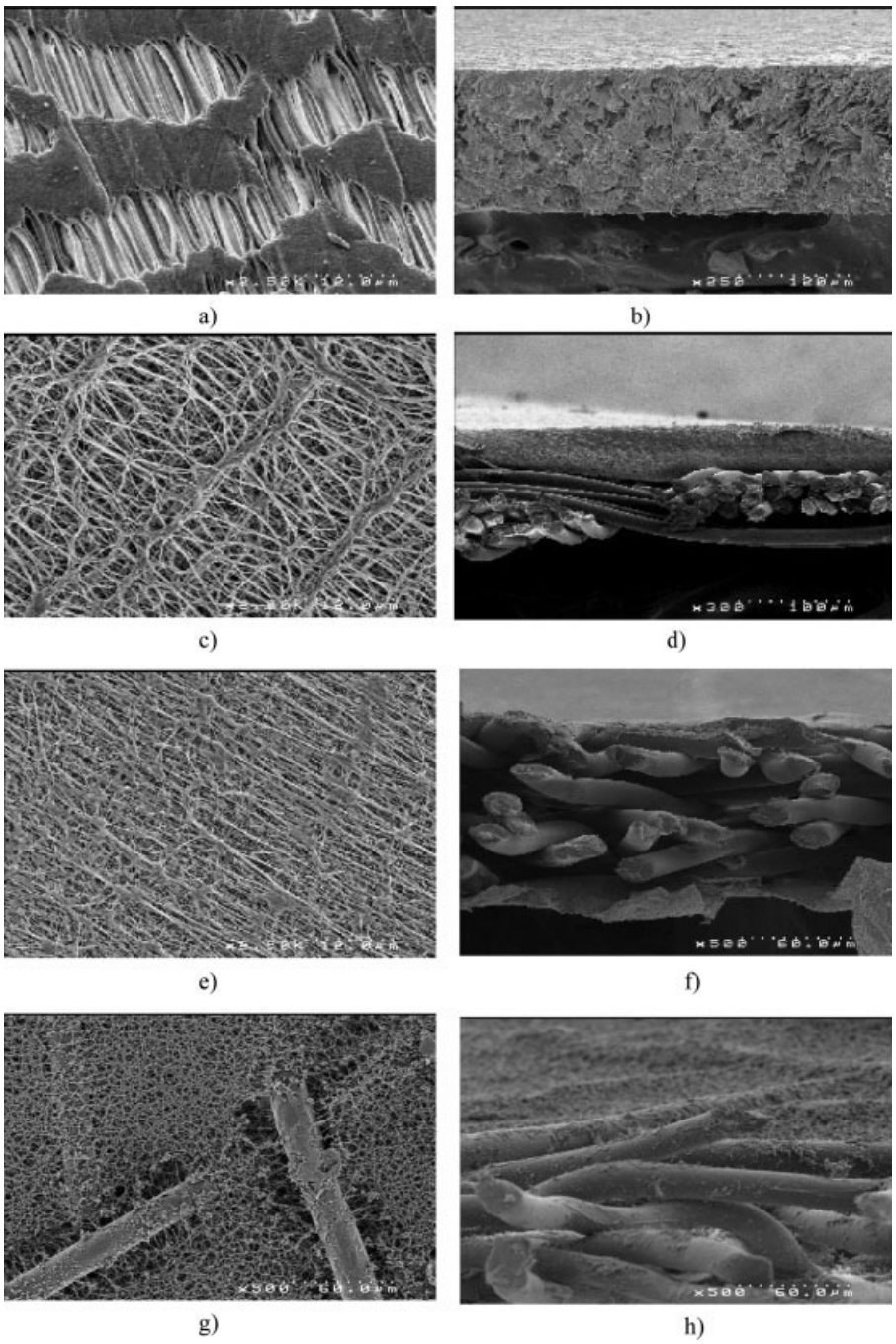

Figure 3. SEM micrographs of membrane 1 surface (a) and cross-section (b); membrane 2 surface (c) and cross-section (d); membrane 3 surface (e) and cross-section (f); membrane 5 surface (g) and cross-section (h).

Table 2. Mean Pore Size and Porosity of the Tested Membranes

Membrane Reference	Mean Pores Diameter of the Separative Layer (μm)	Mean Pores Diameter of the Support (μm)	Porosity (%)
1	2	N/A	55
2	0.8	11	52
3	1	N/A	63
4	1.5	>10	54
5	1	2	57
6	0.3	1	61

Table 3. Measured Liquid Entry Pressure with Distilled Water and Estimated Mean Pore Diameters

Membrane Reference	Measured LEP (Pa)	Estimated Pore Diameter (μm)
1	95,000	1.6
2	220,000	0.9
3	226,000	0.9
4	200,000	1.1
5	72,000	2
6	>500,000	<0.3

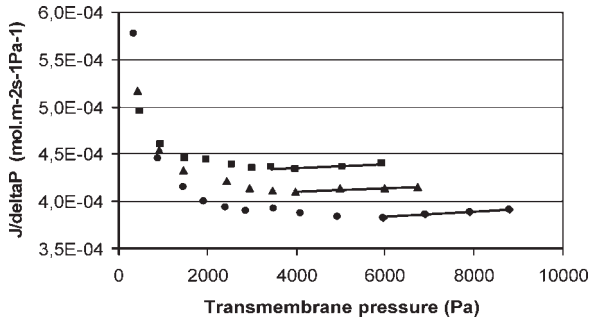

Figure 4. Gas permeance in function of the applied transmembrane pressure for membrane 1 at three different temperatures (■) 25°C, (▲) 40°C, (●) 60°C.

researchers have been developing more explicit forms of this theory which have resulted in the formulation of the DGM reported by Mason and Malinauskas in 1983[14] and described in detail in the theoretical considerations section here below. In the works of Dullien named above,[20,21] as in our case, the mass transport which results on the linear part of the curves, can be considered as a major contribution of convective flow and described by the Hagen-Poiseuille equation (Eq. 1 which results from DGM). This equation can be applied because the transmembrane pressure applied is very low (our experimental transmembrane pressures are ranged between 0 and 9000 Pa) and we can consider that the error contribution by the variation of nitrogen viscosity is also low. Indeed, from Eq. 1, we can estimate the ε/τ parameter:

$$B_0 = \text{slope}^* e = \frac{\varepsilon}{\tau}\frac{r^2}{8\eta}\frac{1}{RT} \tag{1}$$

Table 4 summarizes the values of the estimated ε/τ parameters as well as the values of τ calculated with the porosities measured by mercury intrusion for the six different membranes studied here.

The first four membranes show equivalent properties, which is not surprising as the same technology is used to manufacture them (expanded PTFE). We can observe that tortuosity values are relatively high if we consider that these membranes have a fibrous structure however we should not forget that this is a rough estimated value which is a whole contribution of support and separative layers and the complexity of the multilayered material can be responsible for this relatively high value of the estimated tortuosity. On the contrary, membranes 5 and 6 show a high ε/τ ratio and low tortuosity value. This observation can be explained by a less good control of the separative layer manufacturing resulting in preferential ways of transport as it can be seen in SEM observations (Figure 3g).

Theoretical Considerations

Mass transfer model

In the present work, DGM[14,22] has been used to describe mass transfer through the porous membrane. This model is based on the idea of considering the solid phase (the membrane) as large molecules ("dust") in a multicomponent gas mixture in order to be able to describe the complex combination of viscous flow, Knudsen diffusion and molecular diffusion in a porous media. In this work, we deal with macroporous membranes; indeed, the DGM seems to be the best model to describe the global mass transfer.

Viscous flow is bulk; nonseparating flow caused by total pressure gradients, whereas in the Knudsen regime the transport is controlled by molecule-wall interactions. Moreover, molecule-molecule interactions define the molecular (ordinary or continuum) diffusion.

In its general form, the DGM for component "i" in a mixture of n components is expressed by the following relationship[14,22]:

$$\frac{RT}{D_{iK}}J_i + \sum_{j=1}^{n}\left[\frac{RT}{D_{ij}}(x_j J_i - x_i J_j)\right] = -\nabla p_i - \frac{x_i}{D_{iK}}\frac{B_0 p}{RT\mu}\nabla p \tag{2}$$

where D_{iK} and D_{ij} are the effective Knudsen and molecular diffusion coefficients, respectively, given as:

$$D_{iK} = \frac{4}{3}K_0 v_{Mi} \tag{3}$$

$$D_{ij} = \frac{\varepsilon}{\tau}D_{ij}^* \tag{4}$$

v_{Mi} is the mean molecular speed of the gas molecules of component i and D_{ij}^* is the intrinsic binary diffusion coefficient. (For additional notation, see the list of symbols at the end of the article.)

The structure of the porous medium is described by three morphological parameters. B_0 adjusts the viscous flow term on the right hand side of Eq. 2. It is characteristic of the medium and independent of the gas used. K_0 is the morphological parameter of the Knudsen diffusion coefficient and depends primarily on the morphology of the medium, but also slightly on the absolute pressure and gas nature. These values were estimated making the assumption of tortuous, monodispersed capillaries, which neither are interconnected, nor change their cross-sectional area with their length so K_0 and B_0 can be expressed as:

$$K_0 = \frac{\varepsilon}{\tau}\frac{d_p}{4} \tag{5}$$

$$B_0 = \frac{\varepsilon}{\tau}\frac{d_p^2}{32} \tag{6}$$

The third morphological parameter is the effective porosity/tortuosity ratio, ε/τ, which adjusts the continuum diffusion

Table 4. Gas Permeation Measurements Results

Membrane Reference	ε/τ	τ
1	0.24	2.4
2	0.23	1.9
3	0.22	2.8
4	0.18	2.9
5	0.57	1.0
6	0.48	1.3

coefficient to the structure of the porous medium. It is important to notice that $D_{i\mathrm{K}}$ describes not only Knudsen diffusion but also the contribution of slip flow along the pore walls in the transition region between Knudsen diffusion and continuum transport.

The main assumptions taken for this model are:

- Ideal gas behavior.
- Air is considered as a binary mixture of dry air and water vapor.
- The properties of the membrane are perfectly homogeneous.

For the case of a binary mixture of components A and B, the "DGM" can be reduced for component A to the following equation:

$$J_{\mathrm{A}} = S\left(-\frac{D_{\mathrm{B}}}{R\cdot T}\cdot\frac{\delta_{\mathrm{A}}\cdot x_{\mathrm{A}}}{(1-\delta_{\mathrm{A}}\cdot x_{\mathrm{A}}-\delta_{\mathrm{B}}\cdot x_{\mathrm{B}})}\cdot\nabla_p - \frac{1}{R\cdot T}\right.$$
$$\left.\times\frac{D_{\mathrm{A}}\cdot(1-\delta_{\mathrm{B}}\cdot x_{\mathrm{B}})-D_{\mathrm{B}}\cdot\delta_{\mathrm{A}}\cdot x_{\mathrm{A}}}{(1-\delta_{\mathrm{A}}\cdot x_{\mathrm{A}}-\delta_{\mathrm{B}}\cdot x_{\mathrm{B}})}\cdot\nabla p_{\mathrm{A}} - x_{\mathrm{A}}\cdot\frac{B_0\cdot p}{R\cdot T\cdot\mu}\cdot\nabla p\right) \tag{7}$$

where D_{A} and δ_{A} are the parameters used to compare the influence of Knudsen diffusion and slip flow with the molecular diffusion on permeability, they are given, respectively, as:

$$D_{\mathrm{A}} = \left(\frac{1}{D_{\mathrm{AB}}}+\frac{1}{D_{\mathrm{AK}}}\right)^{-1} \tag{8}$$

$$\delta_{\mathrm{A}} = \frac{D_{\mathrm{A}}}{D_{\mathrm{AB}}} \tag{9}$$

δ_{A} is equal to 1 when molecular diffusion is the only transport phenomenon considered through the membrane pores. The first two terms of the right-hand side of the Eq. 7 represent the diffusive transfer (Knudsen and molecular) through the membrane. The last term is related to convection. Then, Eq. 7 can then be written according to these two terms:

$$J_{\mathrm{A}} = S\left(k_{\mathrm{A,mem}}\times\Delta p_{\mathrm{A}} - x_{\mathrm{A}}\times\frac{B_0\times P_{\mathrm{T}}}{R\times T\times\mu}\times\nabla p\right) \tag{10}$$

where $k_{\mathrm{A,mem}}$ is the term corresponding to all diffusive phenomena:

$$k_{\mathrm{A,mem}} = -\frac{D_{\mathrm{B}}}{R\times T\times e}\times\frac{\delta_{\mathrm{A}}}{(1-\delta_{\mathrm{A}}\times x_{\mathrm{A}}-\delta_{\mathrm{B}}\times x_{\mathrm{B}})}$$
$$-\frac{1}{R\times T\times e}\times\frac{D_{\mathrm{A}}\times(I-\delta_{\mathrm{B}}\times x_{\mathrm{B}})-D_{\mathrm{B}}\times\delta_{\mathrm{A}}\times x_{\mathrm{A}}}{(I-\delta_{\mathrm{A}}\times x_{\mathrm{A}}-\delta_{\mathrm{B}}\times x_{\mathrm{B}})} \tag{11}$$

This approach considers only the impact of the membrane on mass transport coefficient neglecting the influence of boundary layers and the geometry of the membrane support. Therefore, it is essential to complete this approach by coupling the DGM to a classical in series-resistances model to globally characterize the system and to take into account all the parameters and phenomena which can enhance or slow down the mass transport.

The gas permeation of different components of the gas mixture may generate concentration boundary layers on both sides of the membrane. In fact, the gas permeation creates a negative gradient of partial pressure of the different components which reduces the mass transfer. These effects correspond to the polarization phenomena by concentration (represented in Figure 5) which can have a big impact on the diffusive term of gas permeation.[12] The diffusive permeation coefficient (k_{A}) can then be written as the inverse of the sum of the inverse of the different mass transfer coefficients (equivalent to the conductance in an electronic in-series resistances system).

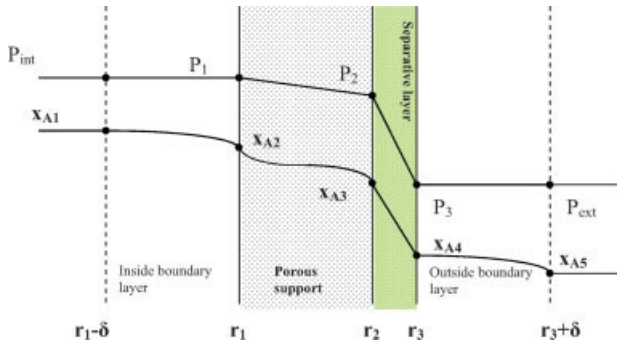

Figure 5. Schematic illustration of the membrane and surroundings described by the resistances in series model.

[Color figure can be viewed in the online issue, which is available at www.interscience.wiley.com.]

$$k_{\mathrm{A,tot}} = \frac{1}{R_{\mathrm{A,tot}}} = \left(\frac{1}{k_{\mathrm{bl,int}}}+\frac{1}{k_{\mathrm{A,mem}}}+\frac{1}{k_{\mathrm{bl,ext}}}\right)^{-1} \tag{12}$$

The contribution of the boundary layers is determined by the calculation of the Sherwood dimensionless number. To obtain the correlations for outside and inside of the walls of the box we can consider the works of Levenspiel[23] for a laminar flow over a plane plate (Eq. 13) and of Acevedo et al.[24] for a natural convection flow within a rectangular enclosure using Chilton-Colburn analogy (Eq. 14):

$$Sh_{\mathrm{ext}} = 0.664Re^{1/2}Sc^{1/3} = \frac{k_{\mathrm{bl,ext}}\cdot d_{\mathrm{h}}\cdot M_{\mathrm{air}}\cdot P_{\mathrm{m}}}{D^*_{ij}\cdot\rho_{\mathrm{air}}} \tag{13}$$

$$Sh_{\mathrm{int}} = 1.5(Grm_{\mathrm{int}}\cdot Sc_{\mathrm{int}})^{1/4} = \frac{k_{\mathrm{bl,int}}\cdot d_{\mathrm{h}}\cdot M_{\mathrm{air}}\cdot P_{\mathrm{m}}}{D^*_{ij}\cdot\rho_{\mathrm{air}}} \tag{14}$$

The diffusion coefficient of water vapor in dry air at various pressures and temperatures can be estimated with the following empirical relation derived by Massman[25]:

$$D^*_{\mathrm{A,B}} = 2.178\times10^{-4}\frac{P_0}{P_T}\left(\frac{T}{273.15}\right)^{1.81} \tag{15}$$

where P_0 is the atmospheric pressure (1.013bar = 1.013×10^5 Pa).

Heat transfer model

The modeling and simulation of temperature evolution during transient states were carried out taking into account

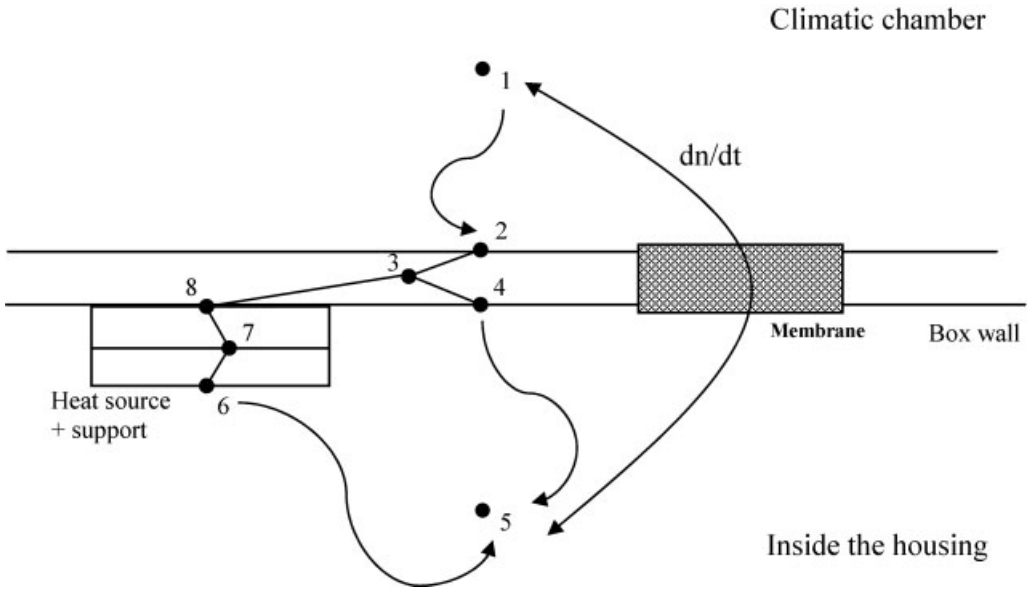

Figure 6. Mesh considered for heat transfer model.

all the parameters related to heat conduction resistances and calorific capacities of the box walls and PCB installed inside. Calculations were carried out considering the mesh approach shown in Figure 6. The model equations for thermal transport phenomena are available with and without mass transfer and consider all important heat transfer modes available in and along the box and the membrane, only radiation was not considered in this approach. Boundary and initial conditions are expressed in general way and can be varied depending on considered experimental conditions.

Conservative heat transfer equation is written at every node of the meshing leading to seven equations describing the temperature evolution of every node (we consider that temperature at node 1 is known):

Equation at node 2: continuity at the external box wall surface:

$$\alpha_{\text{ext}} \cdot S_{\text{box}} \cdot (T_1 - T_2) = \frac{\lambda_{\text{box}} \cdot S_{\text{box}}}{z_{\text{box}/2}} \cdot (T_2 - T_3) \qquad (16)$$

here $\alpha_{\text{ext}} \cdot S_{\text{box}} \cdot (T_1 - T_2)$ is the heat power transmitted by forced convection between the surface of the box and the air outside the box and $\frac{\lambda_{\text{box}} \cdot S_{\text{box}}}{z_{\text{box}/2}} \cdot (T_2 - T_3)$ is the heat power transferred by conduction between the outside surface of the box and node 3 (half thickness)

Equation at node 3: internal heating of the box wall:

$$\frac{dT_3}{dt} \cdot m_{\text{box}} \cdot C_{\text{p,box}} = \frac{\lambda_{\text{box}} \cdot S_{\text{box}}}{z_{\text{box}/2}} \cdot (T_2 - T_3) + \frac{\lambda_{\text{box}} \cdot (S_{\text{box}} - S_{\text{metal}})}{z_{\text{box}/2}} \cdot (T_4 - T_3) + \frac{\lambda_{\text{box}} \cdot S_{\text{metal}}}{z_{\text{box}/2}} \cdot (T_8 - T_3) \qquad (17)$$

here $\frac{dT_3}{dt} \cdot m_{\text{box}} C_{\text{p,box}}$ is the power accumulated by the box material (specific heat capacity). Other terms represent the participation by conduction of the box material between node 3 and respectively the outside surface of the box, the inside surface of the box and the interface (heat source-inside surface of the box).

Equation at node 4: Continuity at the internal box wall surface:

$$\alpha_{\text{int,box}} \cdot (S_{\text{box}} - S_{\text{metal}}) \cdot (T_4 - T_5) = \frac{\lambda_{\text{box}} \cdot (S_{\text{box}} - S_{\text{metal}})}{z_{\text{box}/2}} \times (T_3 - T_4) \qquad (18)$$

In the aforementioned equation $\alpha_{\text{int,box}} \cdot (S_{\text{box}} - S_{\text{metal}}) \cdot (T_4 - T_5)$ represents the heat exchanged by natural convection between inside surface of the box and internal air.

Equation at node 5: Internal air heating:

$$\frac{dT_5}{dt} \cdot \sum n_i \cdot C_{\text{p},i} = \alpha_{\text{int,box}} \cdot (S_{\text{box}} - S_{\text{metal}}) \cdot (T_4 - T_5) + \alpha_{\text{int,metal}} \cdot S_{\text{metal}} \cdot (T_6 - T_5) + (T_1 - T_5) \cdot \sum \frac{dn}{dt} \cdot C_{\text{p},i} \qquad (19)$$

here $\frac{dT_5}{dt} \cdot \sum n_i \cdot C_{\text{p},i}$ is the heat accumulated by the different components of inner air due to their specific heat capacities and $(T_1 - T_5) \cdot \sum \frac{dn}{dt} \cdot C_{\text{p},i}$ is the heat transferred by the mass transfer of air and water vapor through the membrane.

Equation at node 6: Continuity at the interface (heat source-internal air):

$$\alpha_{\text{int,metal}} \cdot S_{\text{metal}} \cdot (T_5 - T_6) = \frac{\lambda_{\text{metal}} \cdot S_{\text{metal}}}{z_{\text{box}/2}} \cdot (T_6 - T_7) \qquad (20)$$

Equation at node 7: Heat generation:

$$\frac{dT_7}{dt} \cdot m_{\text{metal}} \cdot C_{\text{p,metal}} = \frac{\lambda_{\text{metal}} \cdot S_{\text{metal}}}{z_{\text{box}/2}} \cdot (T_6 - T_7) + \frac{\lambda_{\text{metal}} \cdot S_{\text{metal}}}{z_{\text{box}/2}} \cdot (T_8 - T_7) + Q_{\text{electr}} \qquad (21)$$

here $\frac{dT_7}{dt} \cdot m_{\text{metal}} \cdot C_{\text{p,metal}}$ represents the heat power accumulated by the heat source support (specific heat capacity) and Q_{electr} represents the power dissipated by the heat source.

Equation at node 8: Continuity at the interface (box wall-heat source support)

$$\frac{\lambda_{\text{metal}} \cdot S_{\text{metal}}}{z_{\text{metal}/2}} \cdot (T_7 - T_8) = \frac{\lambda_{\text{box}} \cdot S_{\text{metal}}}{z_{\text{metal}/2}} \cdot (T_8 - T_3) \qquad (22)$$

Different assumptions are considered in these equations:

Heat conduction through the membrane is negligible (the membrane surface and its thermal conductivity are very small when we compared, respectively, to the total box surface and the metal thermal conductivity).

- Internal air has a unique (homogeneous) temperature (T_5) far from the enclosure wall.
- The internal temperature of the box wall (T_3) is homogeneous.

The coefficients $\alpha_{\text{int,box}}$, $\alpha_{\text{int,metal}}$, α_{ext}, used to describe the heat transfer by convection between the walls and the air, are calculated according to the type of existing convection:

- Inside the box, only natural convection has to be taken into account as the only phenomena creating air motion is the gradient of temperature.
- Outside the box, forced convection is taking place due to the presence of a fan in the climatic chamber or to the movement of the car.

An adequate equation describing forced convection of air on a flat plate using dimensionless numbers has been developed by Eyglunent,[26] it is given here below:

$$Nu = 0.024 \cdot Re^{0.805} = \frac{\alpha_{\text{ext}} \cdot X_{\text{ext}}}{\lambda_{\text{box}}} \qquad (23)$$

This equation is only valid for low values of Re and Nu ($Re < 10^5$, $Nu < 2 \times 10$).

For natural convection, a good correlation is also given by Eyglunent[26]:

$$Nu = \frac{\alpha_{\text{int,box}} \cdot X_{\text{int,box}}}{\lambda_{\text{box}}} \qquad (24)$$

$$Nu = \frac{\alpha_{\text{int,metal}} \cdot X_{\text{int,metal}}}{\lambda_{\text{metal}}} \qquad (25)$$

With

$$Nu = 0.59 \cdot (Gr \cdot Pr)^{1/4} \qquad (26)$$

$$Gr = \frac{g \cdot \beta \cdot \Delta T \cdot \rho^2 \cdot {d_{\text{h}}}^3}{\mu^2} \qquad (27)$$

$$Pr = \frac{C_{\text{p}} \cdot \mu}{\lambda} \qquad (28)$$

The coefficient 0.59 and [1/4] can only be applied for a value of $Gr.Pr$ included in the interval [10^4–10^9] which is true in our case.

This approach takes into account all the phenomena interfering with the change of temperature inside the box in transient and steady state conditions.

Equation 19 shows a term depending on mass transfer parameters (dn/dt) so the heat transfer model cannot be complete without coupling it to mass transfer model. In fact, as far as we have a membrane, rapid mass transfer takes place with pressure, and then, air temperature inside the box can be strongly influenced.

The calculation of the coupling of heat and mass transport models has been carried out with Matlab® software to draw simulation curves showed below in the next section. All necessary data and parameters for the calculations were obtained experimentally and from literature, they are given in Table 5.

Results and Discussion

Comparison between simulation and experimental results

To validate the model, we carried out series of experiments with electronics housings described in the "Experimental set-up with an actual electronics housing" subsection of the second section. As explained earlier in the experimental section, the conditions (% RH, temperature) considered of the climatic chamber were chosen according to the French automotive industry regulations. As discussed in the previous section, all simulation results were obtained by the simultaneous resolution of Eqs. 3–15 for two components A (dry

Table 5. Data Used for Calculations

Model Input	Used Equation or Value	Units	Reference
Mass transfer			
Diffusion coefficient	$D^*_{\text{A,B}} = 2.178 \times 10^{-4} \frac{P_0}{P_T} \cdot \left(\frac{T}{273.15}\right)^{1.81}$	$m^2\ s^{-1}$	Massman [25]
Mean molecular speed	$\sqrt{8RT/\pi.M_{\text{A}}}$	$m\ s^{-1}$	Mulder [17]
Air Velocity (outside the box)	4	$m\ s^{-1}$	Measured in this work
Heat transfer			
Density of the metal	Aluminum alloy (1st Box): 2700 Stainless steel 316S (2nd Box): 7990	$kg\ m^{-3}$	Perry and Green [27]
Conductivity of the metal	Aluminum alloy:237 Stainless steel 316S: 16.2	$W\ m^{-1}\ K^{-1}$	Perry and Green [27]
Heat capacity of the metal	Aluminum alloy: 903 Stainless steel 316S: 500	$J\ kg^{-1}\ K^{-1}$	Perry and Green [27]
Conductivity of air	$\lambda_{\text{A}} = 7.5536\times10^{-5}\times T + 0.00343$	$W\ m^{-1}\ K^{-1}$	McCabe et al. [28]
Conductivity of water vapor	$\lambda_{\text{B}} = 5.0214\times10^{-5}\times T + 0.00418$	$W\ m^{-1}\ K^{-1}$	McCabe et al. [28]
Heat capacity of air	$Cp_{\text{A}} = 4.19\times(6.386 + 1.762\times10^{-3}\times T - 0.2656\times10^{-6}\times T^2)$	$J\ kg^{-1}\ K^{-1}$	McCabe et al. [28]
Heat capacity of water vapor	$Cp_{\text{B}} = 4.19\times(8.22 + 1.5\times10^{-4}\times T + 1.34\times10^{-6}\times T^2)$	$J\ kg^{-1}\ K^{-1}$	McCabe et al. [28]
Viscosity of air	$\mu_{\text{A}} = 1.71\times10^{-5}.\left(\frac{T}{273}\right)^{2/3}$	Pa s	Williams [29]
Viscosity of water vapor	$\mu_{\text{B}} = 1.703\times10^{-5}.\left(\frac{T}{273}\right)^{1.04}$	Pa s	Teske et al. [30]

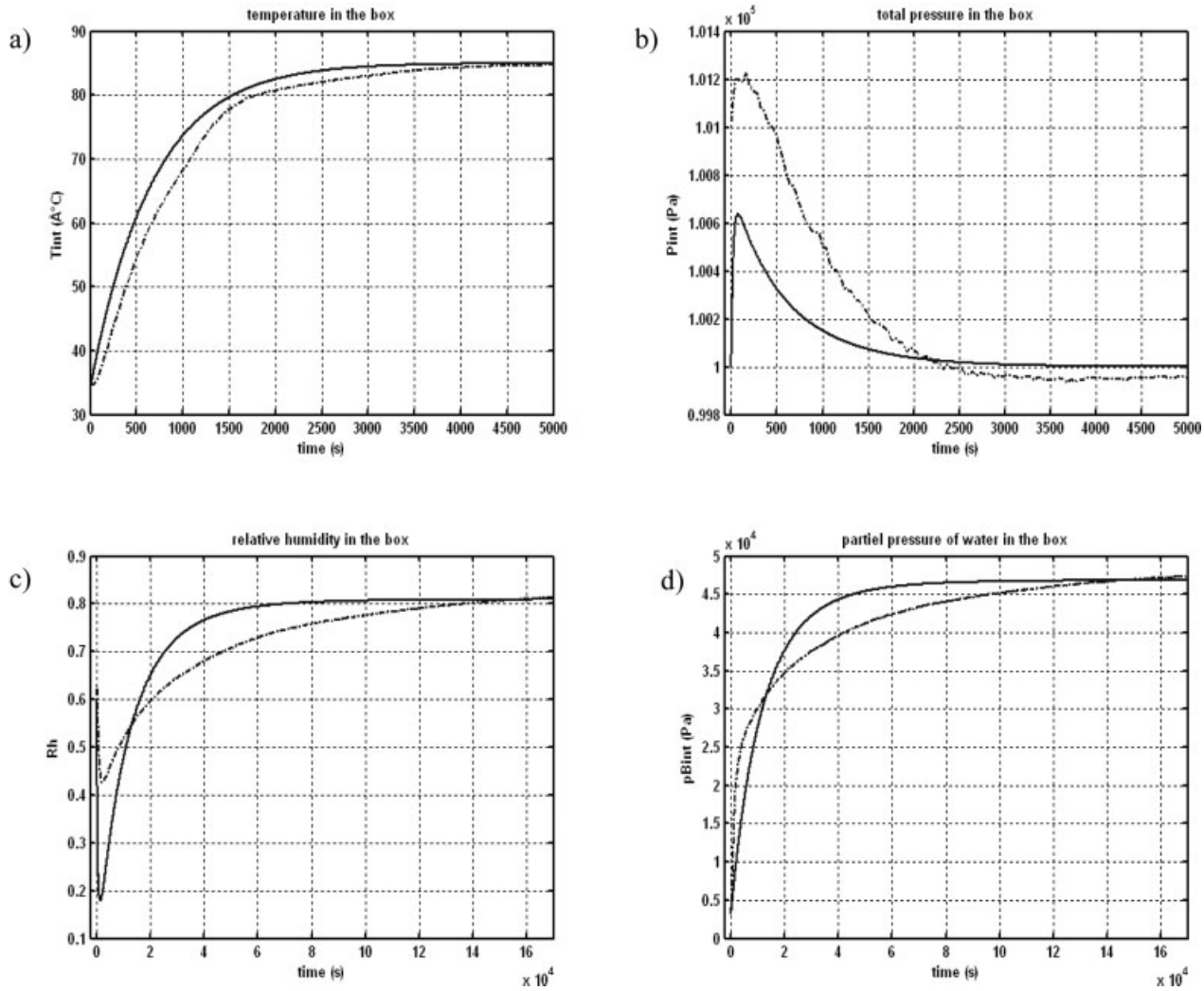

Figure 7. Evolution of environmental parameters inside the actual enclosure with membrane 4 and without heating.

(a) Temperature, (b) Total pressure, (c) relative humidity, (d) water vapor partial pressure (dashed line: experimental results, continuous line: simulation results). Initial conditions inside the box: 35°C, 62% of RH, atmospheric pressure. Imposed environmental conditions: *T*: 85°C, RH: 85%, atmospheric pressure.

air) and B (water vapor) and the thermal Eqs. 16–26 using Matlab® software.

Validation experiments: 85°C, 85% RH outside conditions and without heat dissipation inside the actual housing

For this first validation experiment, we used conditions usually applied in automotive electronic tests to evaluate the limits of the systems. These conditions are considered as the best aging conditions. Therefore, it was important to start the model validation with these parameters to observe the response of the model in those extreme situations. The experiment was carried out with the actual electronics housing, starting at room conditions: initial temperature and RH of 35°C and 61% respectively, a rapid variation of surrounding conditions is applied to reach 85°C and 85% of temperature and RH respectively.

Figure 7 shows a plotting of experimental (dashed line) and simulated (continuous line) evolutions of the internal environmental parameters, which are temperature (*T*), total pressure (*P*), water relative humidity (%RH) and water vapor partial pressure (P_v).

Simulated internal temperature follows very closely the experimental results. Indeed, the thermal approach is precise and the meshing chosen is good enough to consider the delay due to the box material warm up and all heat transfer modes considered.

The internal total pressure increases slightly and the evolution with time of the simulated pressure follows the experimental results. In transient conditions, the measured pressure is a little different from the simulated one. This difference should be due to the error range of the pressure transducer and to the variation of the atmospheric pressure during the test time, this parameter is not taken into account in modeling.

P_v and RH evolution on time fit well experimental results except at the beginning where experimental P_v increases faster than the simulated one whereas the experimental RH decreases less than calculated. This result indicates that appa-

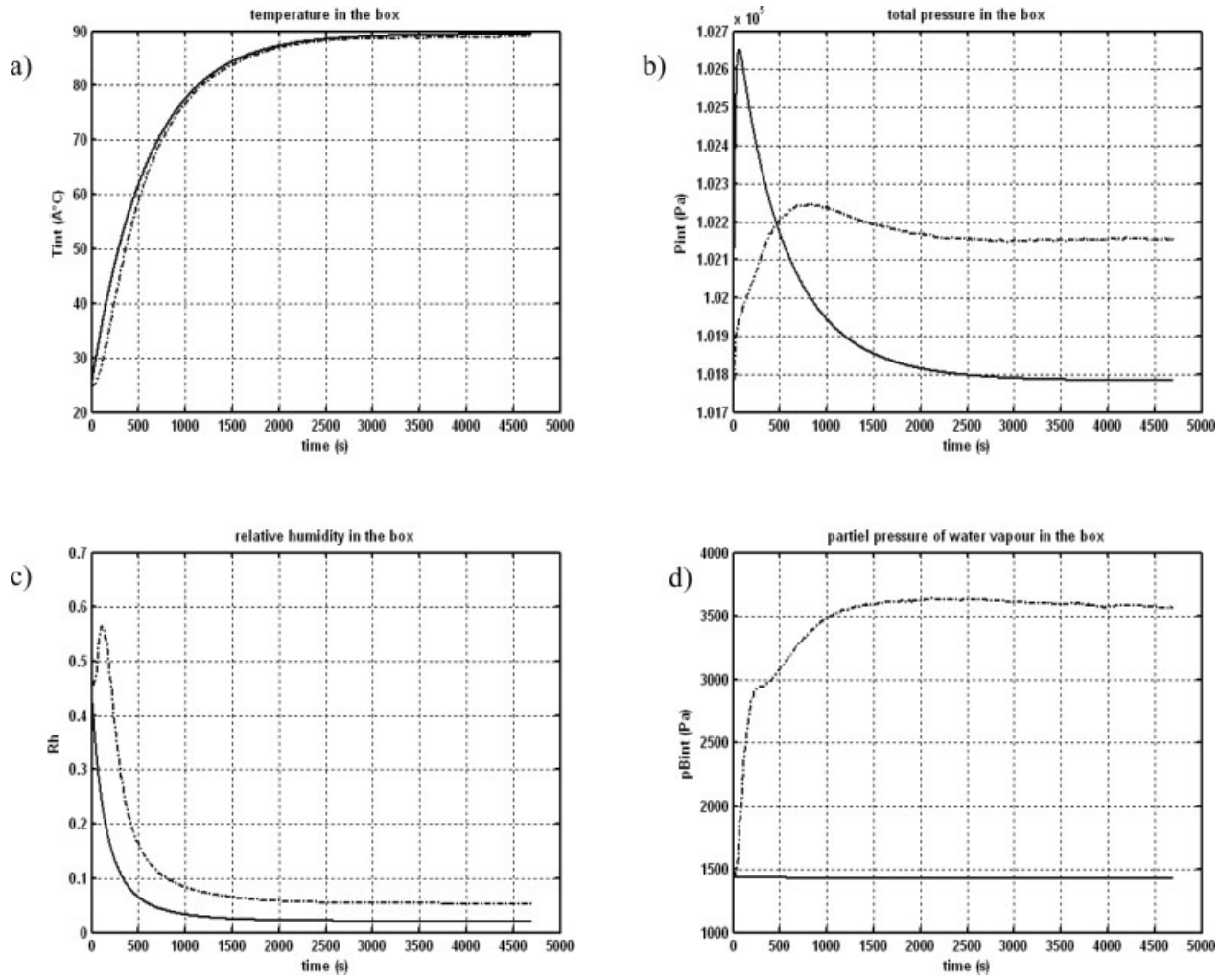

Figure 8. Evolution of environmental parameters inside the actual enclosure with membrane 4 and with a heating source inside (25 W of heat dissipation).

(a) Temperature, (b) Total pressure, (c) relative humidity, (d) water vapor partial pressure. (--) dashed line: experimental results, (—) continuous line: simulation results. Initial conditions inside the box: *T*: 27°C, RH: 46%, atmospheric pressure. Imposed environmental conditions: *T*: 25°C, RH: 45%, atmospheric pressure.

rently other phenomena, which are not considered in the model, may occur. An explanation can be done if we consider that water vapor desorption can take place from polymeric materials of the PCB and the electronic components enclosed in the housing (in this first experiment resistances were not plugged in). Indeed, this desorption phenomena will influence the total P_v. This explanation will be confirmed later by other tests carried out with the polymer-free reference electronics housing.

Validation experiments: 25°C, 45% RH outside conditions and with 25 W of heat dissipation inside the actual box

These conditions are closer to the real function of an ECU and are often met in electronic applications where heat dissipation can be important. Initial conditions inside the box were 27°C, 46% RH (room conditions) and atmospheric pressure. The small variation of these surrounding conditions was very fast compared to the experiment duration (25°C, 45% RH outside).

Figure 8 shows a comparison between experimental and calculated evolution of the environmental parameters inside the box.

As it has been presented in the previous case, calculated temperature evolution fits well the experimental one; this observation corroborates the complete and general aspect of the thermal approach. The total simulated pressure shows a deviation compared to the measured one but the stabilization time is respected. However, it is important to note that the deviation observed is very small when compared with the error range of the pressure transducer (±500 Pa).

Concerning the P_v and the RH, the experimental results are slightly higher than the modeled ones. This result is similar to the aforementioned previous case and a similar explanation about water desorption from polymeric materials can be given. In fact, in this case the impact of desorption is more perceptible because the RH outside the box does not

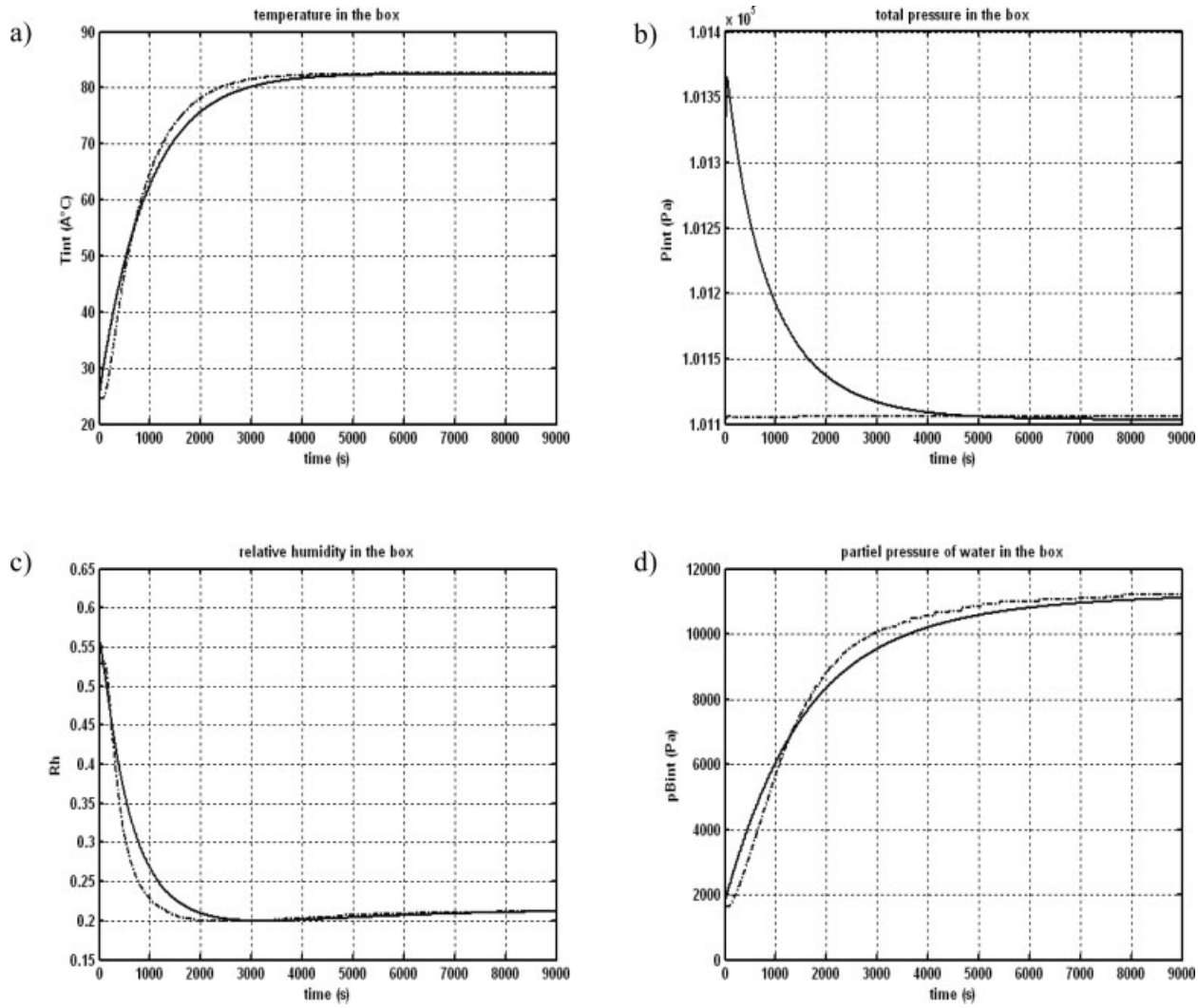

Figure 9. Evolution of environmental parameters inside the reference enclosure with membrane 4 and without heating in: (a) Temperature, (b) Total pressure, (c) relative humidity, (d) water vapor partial pressure (--) dashed line: experimental results, (—) continuous line: simulation results.

Initial conditions inside the box: *T*: 25°C, RH: 55%, atmospheric pressure. Imposed environmental conditions: *T*: 83°C, RH: 20%, atmospheric pressure.

change during the test. Therefore, no water vapor exchange is expected and the only observed variation is due to phenomena taking place inside the box. The created P_v difference is low, so, the kinetics of diffusion through the membrane is slow and the equilibration time is long. However, we can observe that all the studied curves follow the same time dependent evolution.

We can then conclude, a priori, that the modeling of the internal environmental parameters is valid. Nevertheless to confirm our hypothesis of water desorption we carried out validation tests with a home-made housing which is made of 100% of stainless steel.

Reference box validation experiment: 83°C, 20% RH outside conditions

The home-made reference box was build with the objective of having an enclosure with well-known characteristics and with materials which do not adsorb water vapor in the inner compartment. Indeed, all the characteristics of the material used to build up the box and of the membrane (membrane 4) are exactly known. The chosen experiment is different from the first two validation experiments to test the flexibility of the model when changing multiple parameters. Initial conditions were room conditions: 25°C, 55% RH and atmospheric pressure, then housing was introduced in the climatic chamber which was maintained at 83°C and 20% RH. As explained earlier the variation of the surrounding conditions was fast compared to the test duration.

Figure 9 shows the evolution with time of all internal parameters listed previously and obtained results corroborate the validity of the developed model.

In this case pressure calculated with the model does not follow experimental results mainly in the first 3000 s. This behavior can be explained because of the level of error range

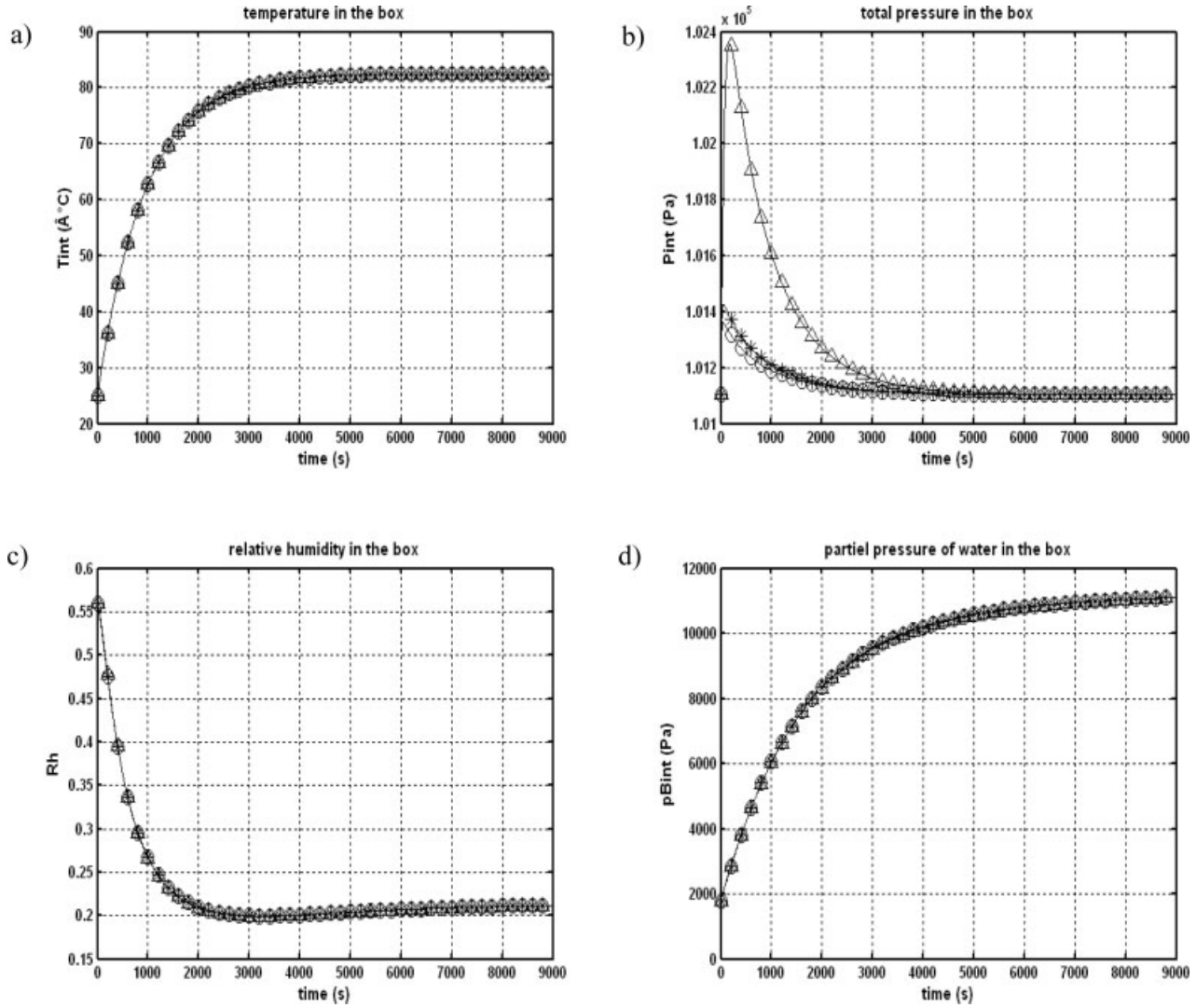

Figure 10. Simulated evolution of environmental parameters inside the enclosure using three different membranes and without electronic heat dissipation. R_s = 0.005.

Initial conditions inside the box: T: 25°C, RH: 55%, atmospheric pressure. Outside conditions: T: 82°C, RH: 21%, atmospheric pressure. -○- membrane 1, -*- membrane 4, -△- membrane 6. (a) Temperature (T), (b) total pressure (P), (c) relative humidity (RH) and (d) water vapor partial pressure (P_v).

of the sensor (±500 Pa) or a little underestimated membrane permeation. In terms of simulated pressure variation we can also note that this variation is lower (less than 300 Pa) than the variation calculated with the actual enclosure (~800 Pa) because the membrane surface is bigger in this last case (3.14×10^{-4} m^2). All the other simulated evolutions: temperature, P_v and RH, fit exactly the experimental results. This test confirms the validation of the model and the hypothesis of water desorption from polymeric materials with the actual housing during the heating up step. Indeed, as the reference box does not enclose any plastics no overshoot on humidity is observed.

Simulation study

Once, we have validated the model we carried out simulations to study the influence of: 1-membrane type and surface, 2-different fluxes contribution to heat transport, 3-boundary layers. All simulation results described here below have been carried out considering that the electronic housing, with internal initial conditions (T: 25°C, P: atmospheric pressure, RH: 56%) was placed in a climatic chamber at 82°C and 21% RH.

Simulations with different membranes

Figure 10 gives simulation results for a box equipped with a membrane surface of 3.14×10^{-4} m^2 which corresponds to a ratio of "membrane surface/housing surface" (R_s) of 0.005 for all different membranes characterized in this work.

First, we can notice that, at the exception of membrane 6 which presents the smallest mean pore size among the tested membranes, no noticeable difference exists, during the transient or steady state, in the evolution of temperature, RH, P_v,

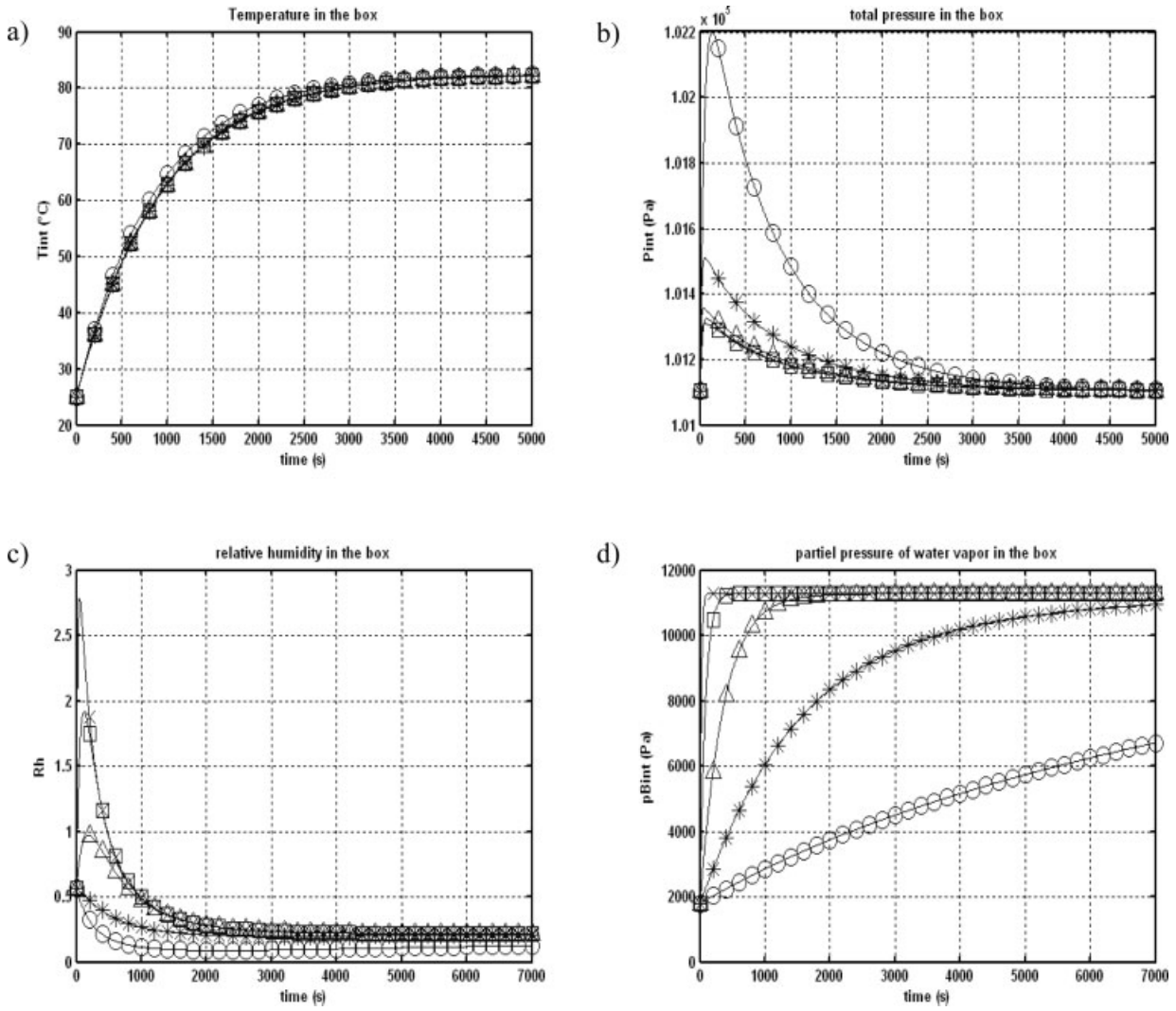

Figure 11. Simulated evolution of environmental parameters inside the enclosure with five different 'membrane surface/metallic box surface' ratios (R_s) -○- R_s = 0.0013, -*- R_s = 0.005, -△- R_s = 0.02, -□- R_s = 0.08, -×- R_s = 0.35.

Membrane 4, outside conditions: 82°C, 21% RH without electronic heat dissipation; initial conditions inside the box: 25°C, 55% of RH and atmospheric pressure. (a) Temperature (T), (b) total pressure (P), (c) relative humidity (RH) and (d) water vapor partial pressure (P_v).

and total pressure. For membrane 6, the calculated overshoot of total pressure inside the box is relatively high when compared with simulations carried out with other membranes. It corresponds to the difference between gas expansion by temperature increase and the relatively low gas flow rate. Nevertheless, we have to consider that this variation is in reality small if we compare it with the experimental results shown in previous sections. In fact errors of experimental pressure measurements are much higher than the calculated variation here. Membranes 1 and 4 show almost the same behavior even if membrane 1 has larger mean pores size. However, the separative layer of membrane 1 is twice as thick as the corresponding layer of membrane 4 and we know that permeation rate is inversely proportional to thickness

In general, we can consider that all macroporous membranes (mean pore size higher than 5×10^{-8} m) are equivalent if we consider the temperature, RH and P_v. Therefore, we decided to continue the simulations considering only membrane 4 characteristics because this membrane had been already chosen for validation tests.

Effect of membrane surface on the evolution of the studied parameters inside the box

To size the chosen membrane for each application, it is important to study the evolution of different environmental parameters inside the box with different membrane dimensions. Thus, we evaluated by simulation five membrane surfaces corresponding to different ratios "membrane surface/housing surface" (R_s) (R_s = 0.0013, 0.005, 0.02, 0.08, and 0.35).

Figure 11 shows the evolution of temperature, total pressure, RH and P_v for the five chosen ratio. Firstly, we can observe that the membrane surface increase has a very small

impact on temperature evolution. Indeed, two opposite phenomena take place: the heat flux increases with mass transfer surface, but at the same time, the heat flux by conduction decreases because the metallic surface of the housing is being reduced. Therefore, we can assume that the membrane plays also a thermal regulation role even if the polymeric material of the membrane has very low intrinsic heat conductivity. The influence of the membrane on the heat transport will be studied in details in the next section.

Secondly, membrane surface has an important influence on total pressure and RH. However the most strongly affected is P_v evolution. Concerning total pressure, we can give the same aforementioned explanation: at low R_s the difference between gas expansion, by temperature increase, and the low gas flow rate explains the behavior observed.

In the case of RH evolution if we exceed a ratio membrane surface/metallic housing surface of 0.02 the mass transport of air at 21% of RH and 85°C is much more rapid than temperature step-up. Indeed, we have a peak of RH inside the box (higher than 1) during the first 1000 s. In those conditions of relatively high membrane surface, condensation takes place immediately on the cold parts of the metallic housing. Therefore, we can notice that a very small membrane surface can be useful in some conditions when the electronics needs a good control of the RH and RH inside the housing to avoid water condensation.

The developed model will help to carry out a dimensioning work and to choose the best membrane size depending on the box specifications (material, size, etc.), the maximum working temperature and the allowed pressure.

Study of the influence of mass transfer on heat transfer

This work aims coupling mass and heat transfer to simulate the environmental internal conditions of electronics housing. As the developed model matches well the experimental results, the importance of the impact of each phenomenon or parameter on other ones, can be evaluated. The impact of heat transfer on the mass transfer is obvious and has been observed in previous simulations, since temperature change will lead to variations of pressure, which is one of the main forces causing the transport of fluid through the membrane. In addition, all mass transfer coefficients also depend on the temperature. However, the influence of the flux of fluid through the membrane on temperature changes in the box is more uncertain. Therefore, the evaluation of the contribution of mass transfer on temperature changes should be simulated to better understand all the phenomena taking place inside the box.

- Study of the different fluxes contribution to heat transfer

To evaluate the importance of the different heat transfer phenomena compared to each other, we decided to simulate the heat flux by conduction through the metal and the heat flux due to the mass transfer through the membrane as a function of time. Here we considered for the simulation T: 25°C, RH: 56% and atmospheric pressure as initial conditions. The surrounding conditions were varied rapidly in a step way to 83°C and 20% RH and keeping atmospheric pressure. This simulation was done considering electronics housing similar to the second reference box at different R_s and with membrane 4 on its surface.

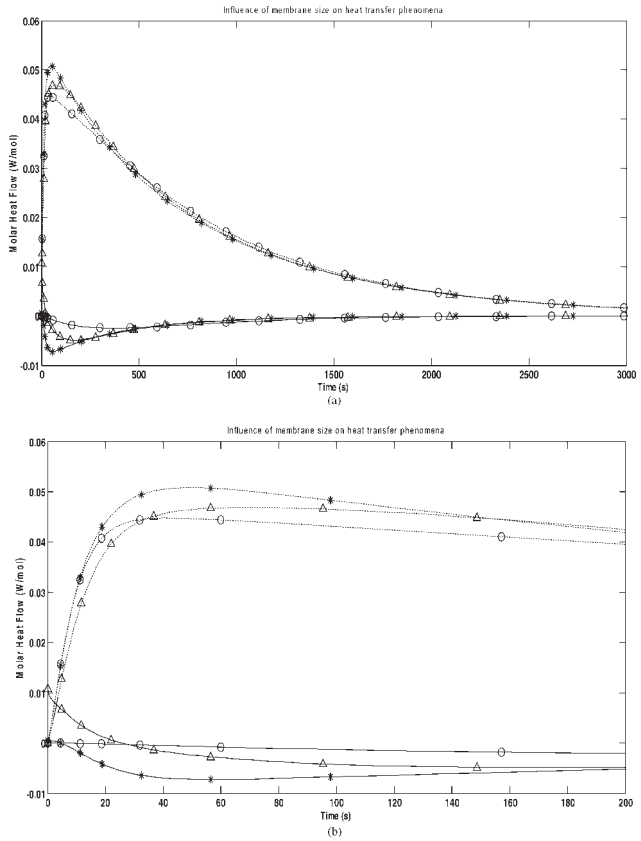

Figure 12. (a) Simulated evolution of different molar heat flows (W/mole of air inside the enclosure): Heat flow due to the mass transport through the membrane (— solid lines). Heat flow by conduction through the wall of the box (-- dashed lines) for three different membrane surface/metal wall surface ratios. (b) Zoom on the first 200 s of Figure (a).

In (a) the membrane surface/metal wall surface ratios: -◯- R_s = 0.0013, -*- R_s = 0.005, -△- R_s = 0.08. Initial conditions in the box: 25°C, 55% of RH, atmospheric pressure. Imposed conditions outside the box: 83°C, 20% of RH and atmospheric pressure.

In Figure 12a we can observe that heat flow due to the mass transfer through the membrane is much lower than heat flow transferred through the walls of the box by conduction, but it should not be neglected. In fact, this flow is opposed to the first one slowing down the heating of the humid air inside the box. We can also notice that the maximum of heat flow due to the mass transfer through the membrane takes place at the same time as the maximum of heat conduction through the wall. This behavior can be explained by the pressure increase under the influence of the heat conduction through the box walls (gas expansion by the temperature increase). Indeed, this created over-pressure allows air convection through the membrane and in consequence, more contribution to the heat loss by mass transfer.

We can observe in Figure 12b that membrane contribution to the heat transfer increases with membrane surface and can even be positive and bigger than heat conduction through the

metallic part of the housing at initial times (if we exceed a certain surface ratio). This result can be explained by the delay introduced by the specific heat capacity of the metal and the high permeation flux that increases with the membrane surface. Indeed, at initial times, the metal warms up before heating the internal air by natural convection; however, the air permeation through the membrane is instantaneous leading to a rapid contribution to the heating of the air inside the box.

These simulation results show that membranes can also play a regulation role of the temperature and can have a positive or negative contribution to the heating of the air inside the housing, this result should also explain the same temperature behavior for different membrane surface/metallic surface ratios (Figure 11a)

- Study of the influence of boundary layers on mass transfer

It is of interest to compare the different existing mass transfer coefficients to evaluate the importance of the boundary layers and membrane on the total air flux. Figure 13 shows the evolution with time of resistances of different layers described in Figure 5. Calculations were made using same initial conditions and parameters used for Figure 12 but with a membrane surface/metal wall surface ratio of 0.08. We can observe that mass transfer resistance inside the box increases with time. This enhancement is almost linear during the first 2500 s and accelerates beyond this time. As it has been shown in previous simulations curves after the instantaneous change of environmental conditions, we have first a high permeation flux through the membrane allowing rapid pressure equilibrium between the inside and the outside of the box; nevertheless, this rapid transfer (1000–1500 s) has not an strong influence on the calculation of the boundary layer resistance. Then, natural convection and diffusion take place inside the box. Therefore, we can reasonably believe that with time and temperature stabilization, diffusion becomes the major transport phenomenon. Thus, we should have a rapid increase of the boundary layer thickness and then, a continuous enhancement of the internal boundary layer resistance, as observed.

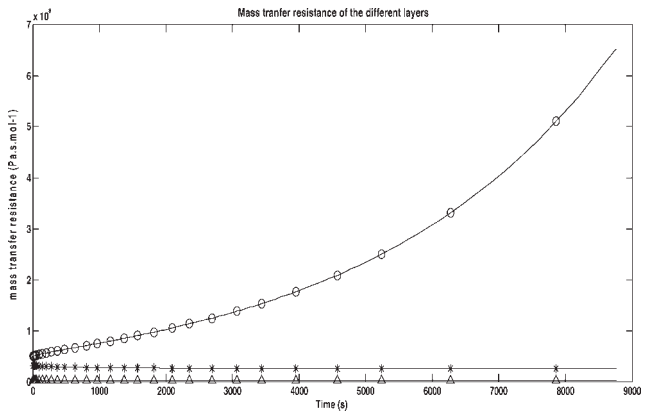

Figure 13. Calculated mass transfer resistances with time: -△- membrane, -*- outside boundary layer and -○- inside boundary layer.

R_s = 0.008. Initial conditions in the box: 25°C, 55% of RH, atmospheric pressure. Conditions outside the box: 83°C, 20% of RH and atmospheric pressure.

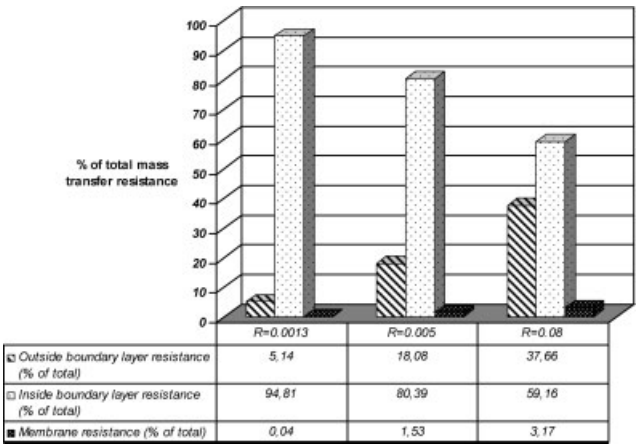

Figure 14. Instantaneous (t = 0) mass transfer resistance of different layers for three surface ratios (R_s = 0.0013, 0.005, 0.08).

Initial conditions in the box: 25°C, 55% of RH, atmospheric pressure. Imposed conditions outside the box: T: 83°C, RH: 20%, atmospheric pressure.

Figure 14 shows the calculation of the relative resistance of boundary layers and membrane for different R_s at time = 0 s. It can be established that for low R_s ratios, the membrane resistance is of little importance for mass transfer between box inner side and surroundings. Indeed, the highest resistance is given by boundary layers and especially inside the box because air movement is very slow and uniquely due to diffusion and natural convection. Therefore, we can conclude that hydrophobic membranes make possible mass transport between the gas inside the box and the surroundings and protect the box inside from liquid water intrusion; but they do not have a strong impact on total mass transfer resistance.

Conclusions

A mathematical model has been developed to investigate the influence of the use of a membrane on electronics housing. This model is based on a complete approach of the mass transfer through a membrane taking into account the effects of boundary layers (concentration polarization). The mass transfer equations were coupled to the heat transfer based on one-dimensional fine meshing. All structural parameters of membranes were determined by different characterization techniques to be introduced into the model.

Theoretical curves obtained fitted well the experimental work, validating then the developed model. The comparison between simulation and experimental results were useful to observe a water desorption phenomenon from plastic materials placed inside the automotive ECU. This phenomenon can have an important influence on the P_v inside the box during the heating up step.

This work allowed the formulation of some other important conclusions:

Firstly, for all tested membranes having pores size in the domain of macroporosity, the total pressure variation inside the box should not exceed 1000 Pa. Indeed, this type of

membrane is efficient for the dynamic and rapid regulation of the total pressure. However, we observed that the evolution of P_v inside the box does not depend on the type of the membrane used because the main resistance to diffusion of water vapor is given by boundary layers and not by the membrane. This effect can only be reduced by increasing significantly the membrane surface, which is not interesting from an industrial point of view. Therefore, any of the tested membranes would be suitable for this application.

Secondly, we showed that membranes have a small role in the heat transfer by conduction as the metallic housing of the box has much higher surface and thermal conductivity. Nevertheless, their impact can not be completely neglected. In fact, for large membrane surfaces heat transfer through the membrane by means of mass transfer can be relatively important, especially at the beginning of the heating step. The metal needs time to get warm due to its specific heat capacity but the gas permeation is instantaneous. We concluded that the membrane in some conditions can also contribute to the temperature regulation inside the box.

Thirdly, because of its mixed contribution to both heat and mass transfer, the membrane controls the RH inside the box. The RH is directly related to the risks of condensation which is one of the major causes of failure in electronics placed inside automotive ECUs.

We proved with the present work that using a venting membrane on electronics housing should be done carefully as it can help internal pressure and temperature regulation but it can accelerate water vapor permeation flux, increasing then the risk of condensation.

The present work will be the basis for a dimensioning work of membranes and the settlement of new rules in the specification book concerning the choice and validation of membranes for electronics housings.

Notation

B_0 = membrane morphological parameter (m^2)
C_p = specific heat (J kg^{-1} K^{-1})
d_h = hydraulic diameter (m)
d_p = pore diameter (m)
D_{ij} = effective diffusion coefficient (m^2 s^{-1})
D^*_{ij} = diffusion coefficient in a binary mixture (m^2 s^{-1})
$D_{i,K}$ = Knudesn diffusion coefficient for a component i (m^2 s^{-1})
e = membrane thickness
Gr = Grashoff number
Grm = mass Grashoff number = $\frac{\rho^2 \cdot g \cdot L^3}{\mu^2} \cdot \frac{\Delta\rho}{\rho}$
g = gravity (9.81 m s^{-2})
J = molar flux density (mol m^{-2} s^{-1})
k = mass transfer coefficient (mol m^{-2} s^{-1} Pa^{-1})
K_0 = membrane morphological parameter (m)
m = weight (kg)
M = molecular weight (kg mol^{-1})
N = Avogadro number (mol^{-1})
Nu = Nusselt number
P = Pressure (Pa)
P_i = Partial Pressure (Pa)
ΔP = Transmembrane pressure (Pa) = $P_{inlet} - P_{outlet}$
P_v = water vapor partial pressure (Pa)
Pr = Pandtl number
Q = heat dissipation power (W)
R = pore radius
R = ideal gas constant (8.314 m^3 Pa $mol^{-1}K^{-1}$)
R_s = membrane surface/metallic surface ratio
RH = Relative humidity (%)
Re = Reynolds number
S = surface (m^2)
Sc = Schmidt number
Sh = Sherwood number
T = Temperature (°C)
v = air velocity (m s^{-1})
x = molar fraction
X = characteristic distance (m)
z = box wall thickness (m)

Greek letters

α = convective heat transfer coefficient (W m^{-2} K^{-1})
β = thermal expansion factor = $\frac{1}{V}\frac{\partial V}{\partial T}$ (K^{-1})
ε = porosity
θ = contact angle (°)
λ = heat conductivity coefficient (W m^{-1} K^{-1})
μ = dynamic viscosity (Pa s)
ν = mean molecular speed (m s^{-1})
ρ = density (kg m^{-3})
τ = tortuosity

Subscripts

A = dry air
air = humid air (A+B)
B = water vapor
box = box wall
ext = outside the box
int = inside the box
m = mean (average)
metal = electronics metallic support
mem = membrane

Literature Cited

1. Ostrach S. Natural convection in enclosures. *J Heat Transfer*. 1988;110:1175–1191.
2. Catton I. Natural convection in enclosures. In: *Proceedings of the Sixth International of Heat Transfer Conference*, Toronto, Canada. 1978;6: 13–31.
3. Yu E, Joshi Y. A numerical study of three-dimensional laminar natural convection in a vented enclosure. *Int J Heat Fluid Flow*. 1997;18:600–612.
4. Nada SA, Moawed M. Free convection in tilted rectangular enclosures heated at bottom wall and vented by different slots-venting arrangements. *J Exp Therm Fluid Sci*. 2004;28:853–862.
5. Khayet M, Matsuura T, Mengual JI, Qtaishat M. Design of novel direct contact membrane distillation membranes. *Desalination*. 2006;192:105–111.
6. Khayet M, Godino P, Mengual JI. Theory and experiments on sweeping gas membrane distillation. *J Memb Sci*. 2000;165:261–272.
7. Romero J. Rios GM. Sanchez J. Bocquet S, Saavedra A. Modelling heat and mass transfer in osmotic evaporation process. *AIChE J*. 2003;49:300–308.
8. Romero J, Rios GM, Sanchez J, Saavedra A. Analysis of sugar boundary layer characteristics and aroma compounds transport in osmotic evaporation. *AIChE J*. 2003;49:2783–2792.
9. Bocquet S, Torres A, Romero J, Sanchez J, Rios G. Modelling the mass transfer in solvent extraction processes with membranes. *AIChE J*. 2005;51:1067–1079.
10. Hengl N, Mourgues A, Pomier E, Belleville MP, Paolucci-Jeanjean D, Sanchez J, Rios G. Study of a new membrane evaporator with a hydrophobic metallic membrane. *J Memb Sci*. 2007;289:169–177.
11. Beuscher U, Gooding CH. The permeation of binary gas mixtures through support structures of composite membranes. *J Memb Sci*. 1998;150:57–75.
12. Mourgues A, Sanchez J. Theoretical analysis of concentration polarisation in membrane modules for gas separation with feed inside the hollow-fibers. *J Memb Sci*. 2005;252:133–144.
13. Martinez L, Florido-Diaz FJ, Hernandez A, Pradanos P. Characterization of three hydrophobic porous membranes used in membrane distillation: modelling and evaluation of their water vapour permeabilities. *J Memb Sci*. 2002;203:15–27.
14. Mason EA, Malinauskas AP. *Gas Transport in Porous Media: The Dusty-Gas Model,* Amsterdam, The Netherlands: Elsevier, 1983.

15. Gibson PW. Effect of temperature on water vapour transport through polymer membrane laminates. *Polym Test*. 2000;19:673–691.
16. Hussain A, Seidel-Morgenstern A, Tsotsas E. Heat and mass transfer in tubular ceramic membranes for membrane reactors. *J Heat Mass Transfer*. 2006;49:2239–2253.
17. Mulder M. *Basic Principles of Membrane Technology*, Twente, The Netherlands: Kluwer, 1991.
18. Garcia-Payo MC, Izquierdo-Gil MA, Fernandez-Pineda C. Wetting study of hydrophobic membranes via liquid entry pressure measurements with aqueous alcohol solutions. *J Colloid Interface Sci*. 2000;230:420–431.
19. Gabino F, Belleville MP, Preziosi-Belloy L, Dornier M, Sanchez J. Evaluation of the cleaning of a new hydrophobic membrane for osmotic evaporation. *Sep Purif Technol*. 2007;55:191–197.
20. Scott DS, Dullien FAL. Diffusion of ideal gases in capillaries and porous solids. *AIChE J*. 1962;8:113–117.
21. Dullien FAL. *Porous Media: Fluid Transport and Pore Structure*. New York, London: Academic Press, 1979.
22. Beuscher U, Gooding C. Characterization of the porous support layer of composite gas permeation membranes. *J Memb Sci*. 1997; 132:213–227.
23. Levenspiel O. *Engineering Flow and Heat Exchange*. New York: Plenum, 1998.
24. Acevedo C, Sanchez E, Young ME. Heat and mass transfer coefficients for natural convection in fruit packages. *J Food Eng*. 2007;80:655–661.
25. Massman WJ. A review of the molecular diffusivities of H_2O, CO_2, CH_4, CO, O_3, SO_2, NH_3, N_2O, NO, and NO_2 in air, O_2 and N_2 near STP. *Atmos Environ*. 1998;31:1111–1127.
26. Eyglunent B. *Manuel de Thermique*. Paris: Hermes Science Publications, 1997.
27. Perry RH, Green DW. *Perry's Chemical Engineers' Handbook*, 7th ed. New York: McGraw-Hill Professional, 1997.
28. McCabe W, Smith J, Harriott P. *Unit Operations of Chemical Engineering*, 6th ed. New York: McGraw-Hill, Science/Engineering/Math, 2000.
29. Williams FA. The effect of temperature on the viscosity of air. *Proc R Soc London*. 1926;110:141–167.
30. Teske V, Vogel E, Bich E. Viscosity measurements on water vapor and their evaluation. *J Chem Eng Data*. 2005;50:2082–2087.

Manuscript received Jan. 23, 2008, revision received Jun. 13, 2008, and final revision received Sept. 11, 2008.